Materials Transactions, Vol. 59, No. 5 (2018) pp. 712 to 716

Martensitic Transformation of Retained Austenite in Ferrite Matrix for Low Alloy Steel

Takayuki Yamashita[1,*], Norimitsu Koga[2] and Osamu Umezawa[2]

[1]*Graduate School of Engineering, Yokohama National University, Yokohama 240-8501, Japan*
[2]*Faculty of Engineering, Yokohama National University, Yokohama 240-8501, Japan*

Martensitic transformation behavior in low-alloy transformation-induced plasticity steels has been studied at 293 K and 193 K. The as-received austenite precipitated in the ferrite matrix satisfied the Kurdjumov–Sachs orientation relationship with the ferrite matrix. The transformed martensite in the ferrite matrix was detected and it commonly exhibited the same orientation as the ferrite matrix. The martensitic transformation was independent of the selection of variant by stress accommodation. Thus, the transformed martensite variant was chosen predominantly to reduce interfacial energy. The transformed martensite may contribute to work-hardening in the ferrite matrix as a harder phase. Further, the transformed martensite at ferrite grain boundaries was due to stress accommodation. The variant achieving the highest Schmid factor in individual austenite was predominantly chosen to introduce slip deformation. [doi:10.2320/matertrans.M2017330]

(Received November 1, 2017; Accepted February 2, 2018; Published March 16, 2018)

Keywords: *martensitic phase transformation, electron backscattering diffraction, Kurdjumov–Sachs orientation relationship*

1. Introduction

Metastable austenite in steels transforms to martensite due to mechanical deformation. The transformation enhances a work-hardening of the steels and improves strength–ductility balance, which is called transformation induced plasticity (TRIP). Low alloy steel containing retained austenite (γ) grains dispersed in the ferrite (α) matrix shows a good strength–ductility balance owing to TRIP effect.[1)] The stability of retained austenite is an important factor to control the mechanical property of TRIP steels, because highly stable austenite transforms to martensite at the late stage of plastic deformation and provides further improvement of the strength–ductility balance.[2)] Morphology,[3)] carbon content[4)] and precipitation site[5)] of austenite, and test temperature[2)] influence the stability of retained austenite. However, few studies on the transformation behavior of individual austenite have been conducted, although individual martensite caused by deformation-induced transformation was studied in metastable austenite steels.[6,7)]

When the austenite and martensite satisfy the Kurdjumov–Sachs orientation relationship (K–S OR), i.e. $(111)\gamma//(110)\alpha$ and $[\bar{1}10]\gamma//[\bar{1}11]\alpha$,[8)] austenite can transform to twenty-four types of martensite in the orientations called variants.[9)] Although the twenty-four variants are randomly generated in the prior austenite under thermal martensitic transformation,[10)] a specific variant is selected under deformation-induced martensitic transformation.[11)] The variant selection under high mechanical driving force in the deformation-induced transformation has been demonstrated.[6)] Furthermore, a simple variant selection model for austempered martensite was proposed, where the martensite variants whose close-packed plane was nearly parallel to the primary or secondary slip planes were selected.[7)] However, it is unclear whether these variant selection models are applicable to TRIP steels.

In this study, a low-alloy TRIP steel containing reverted (retained) austenite in the ferrite matrix and satisfying the K–S OR is investigated. Deformation-induced martensite formed in individual austenite in tension is crystallographically characterized.

*Corresponding author, E-mail: yamashita-takayuki-yz@ynu.jp

2. Experimental Procedure

2.1 Material

First, 0.32C–1.45Si–1.74Mn (in mass%) steel plate was cold-rolled and annealed at 1063 K for 400 s in the $\alpha+\gamma$ region, and thereafter austempered at 673 K for 600 s. The initial volume fraction of retained austenite was 17.2% as measured using X-ray diffraction with Cu-Kα radiation and its carbon content was 1.32 mass% as calculated by eq. (1).[12)]

$$a_\gamma = (0.3553 \pm 0.0001) + (0.00105 \pm 0.00002)C \text{ (at\%)} \quad (1)$$

2.2 Tensile test

Sheet-type test specimens with a gauge length of 30 mm, width of 4 mm, and thickness of 2.5 mm were cut using a wire cut electric discharge machine, where the longitudinal direction was parallel to the rolling direction (RD). The normal direction (ND) surface of specimens was mechanically ground and electrically polished in a solution of perchloric acid and ethanol at 253 K and 31 V for 30 s. The uniaxial tensile test and interrupted test were carried out at the initial strain rate of $2.8 \times 10^{-4}\,s^{-1}$ using a mortar-driven tensile test machine at 293 K (in air) and 193 K (immersed in cooling alcohol). The interrupted strains were chosen as 4%, 8%, and 12% of total elongation (measured with a strain gauge).

2.3 EBSD measurement

Electron back scattered diffraction (EBSD, TSL OIM) technique with a field-emission gun scanning electron microscope (FE-SEM, JEOL JSM7001F) was employed to characterize the crystal orientation of retained austenite. The ND surface of the tensile specimens was observed after interrupted tests and the transverse direction (TD) surface of steel sheets was observed before and after tensile tests. Data were recorded on an area of 47 μm × 47 μm with a beam scanning step of 50 nm. Data points less than 0.1 of confidence index (CI) were omitted as noise.

Table 1 Twenty-four variants in Kurdjumov–Sachs orientation relationship according to Ref. 9).

Variant number	Closed-packed plane parallel	Closed-packed direction parallel	Variant number	Closed-packed plane parallel	Closed-packed direction parallel
01	$(111)\gamma//(011)\alpha$' CP1	$[\bar{1}01]\gamma//[\bar{1}\bar{1}1]\alpha$'	13	$(\bar{1}11)\gamma//(011)\alpha$' CP3	$[0\bar{1}1]\gamma//[\bar{1}\bar{1}1]\alpha$'
02		$[\bar{1}01]\gamma//[\bar{1}1\bar{1}]\alpha$'	14		$[0\bar{1}1]\gamma//[\bar{1}1\bar{1}]\alpha$'
03		$[01\bar{1}]\gamma//[\bar{1}\bar{1}1]\alpha$'	15		$[\bar{1}0\bar{1}]\gamma//[\bar{1}\bar{1}1]\alpha$'
04		$[01\bar{1}]\gamma//[\bar{1}1\bar{1}]\alpha$'	16		$[\bar{1}0\bar{1}]\gamma//[\bar{1}1\bar{1}]\alpha$'
05		$[1\bar{1}0]\gamma//[\bar{1}\bar{1}1]\alpha$'	17		$[110]\gamma//[\bar{1}\bar{1}1]\alpha$'
06		$[1\bar{1}0]\gamma//[\bar{1}1\bar{1}]\alpha$'	18		$[110]\gamma//[\bar{1}1\bar{1}]\alpha$'
07	$(1\bar{1}1)\gamma//(011)\alpha$' CP2	$[10\bar{1}]\gamma//[\bar{1}\bar{1}1]\alpha$'	19	$(11\bar{1})\gamma//(011)\alpha$' CP4	$[\bar{1}10]\gamma//[\bar{1}\bar{1}1]\alpha$'
08		$[10\bar{1}]\gamma//[\bar{1}1\bar{1}]\alpha$'	20		$[\bar{1}10]\gamma//[\bar{1}1\bar{1}]\alpha$'
09		$[\bar{1}\bar{1}0]\gamma//[\bar{1}\bar{1}1]\alpha$'	21		$[0\bar{1}\bar{1}]\gamma//[\bar{1}\bar{1}1]\alpha$'
10		$[\bar{1}\bar{1}0]\gamma//[\bar{1}1\bar{1}]\alpha$'	22		$[0\bar{1}\bar{1}]\gamma//[\bar{1}1\bar{1}]\alpha$'
11		$[011]\gamma//[\bar{1}\bar{1}1]\alpha$'	23		$[101]\gamma//[\bar{1}\bar{1}1]\alpha$'
12		$[011]\gamma//[\bar{1}1\bar{1}]\alpha$'	24		$[101]\gamma//[\bar{1}1\bar{1}]\alpha$'

2.4 Variant selection analysis

The variants of martensite were determined by a pole figure method[9] based on the orientation data by EBSD for individual retained austenite and transformed martensite, where the relationship of the close packed plane and direction between austenite and martensite in the Ref. 9) was adopted as listed in Table 1. The variant selection due to mechanical driving force and slip plane was evaluated. The mechanical driving force, U, is calculated by the eq. (2),[6]

$$\mathrm{U} = 1/2\sigma\{\gamma_0 \sin 2\theta + \varepsilon_0(1 + \cos\theta)\} \quad (2)$$

where σ is the tensile stress, γ_0 is the transformation shear strain component parallel to the habit plane with martensitic transformation, ε_0 is the transformation normal strain component acting normal to the habit plane, and θ is the angle between the stress axis and the normal to the habit plane. As the stress applied during the transformation cannot be determined, the mechanical driving force per tensile stress, U/σ, is adopted. The variant exhibiting the highest mechanical driving force is readily selected and it accommodates the tensile strain. However, the model of variant selection by slip plane was also considered in which the martensite variant with the habit plane nearly parallel to the primary or secondary slip plane of austenite was selected.[7] In other words, the variant nucleates preferentially on the slip planes with high Schmid factor in austenite. Subsequently, the Schmid factor for individual variants was evaluated regardless of whether the variant selection by slip plane was successful in retained austenite.

3. Results and Discussion

3.1 Microstructure

Figure 1 shows the microstructure of the as-received (cold-rolled, annealed and austempered) steel sheet on the TD plane. The microstructure consists of ferrite, bainite, and retained austenite as shown in Fig. 1(a). The retained austenite grains forming as island, plate, or block were distributed in both ferrite and bainite regions. The crystal orientation coordinate of the inverse pole figure (IPF) orientation map is normal to the RD in Fig. 1(b), and the ferrite/austenite boundaries are denoted by the red line. A few types of austenite with different crystal orientations appeared in the ferrite region, whereas every austenite in the bainite region showed the same crystal orientation. The retained austenite grain satisfied the K–S OR with the ferrite matrix, where $\{111\}\gamma$ was parallel to $\{110\}\alpha$, and $\langle 110\rangle\gamma$ was parallel to $\langle 111\rangle\alpha$. The pole figures in Figs. 1(c) and (d) show that $(111)\gamma$ overlaid $(101)\alpha$ and $[\bar{1}10]\gamma$ overlaid $[\bar{1}11]\alpha$ in the ferrite region for the variant indicated by square in Fig. 1(b), respectively. The other two variants indicated by arrows in Fig. 1(b) also satisfied the K–S OR as $(\bar{1}\bar{1}\bar{1})\gamma//(\bar{1}10)\alpha$, $[1\bar{1}0]\gamma//[\bar{1}11]\alpha$, and $(\bar{1}\bar{1}1)\gamma//(\bar{1}01)\alpha$, $[0\bar{1}\bar{1}]\gamma//[111]\alpha$. Moreover, the retained austenite in the bainite region, e.g., that surrounded by a solid line in (a), also satisfied the K–S OR with the bainitic ferrite matrix.

3.2 Precipitation of austenite

Figure 2 represents the ferrite/pearlite microstructure as cold-rolled (before annealed) TRIP steel sheet on the ND plane. Fragmented cementite and isolated pearlite, and deformation bands were observed in the ferrite matrix. The pearlite region preferentially transformed to austenite during annealing at the temperature of ferrite + austenite region, and thereafter, a part of the austenite transformed to bainite during austempering. The untransformed austenite finally remains at room temperature after austempering. Therefore, the retained austenite grains in the bainite region reveal the same crystal orientation and K–S OR with the bainite, because the bainitic ferrite satisfies K–S OR with the untransformed austenite grain.[13] However, the ferrite could be fully recovered or recrystallized during annealing at the temperature of

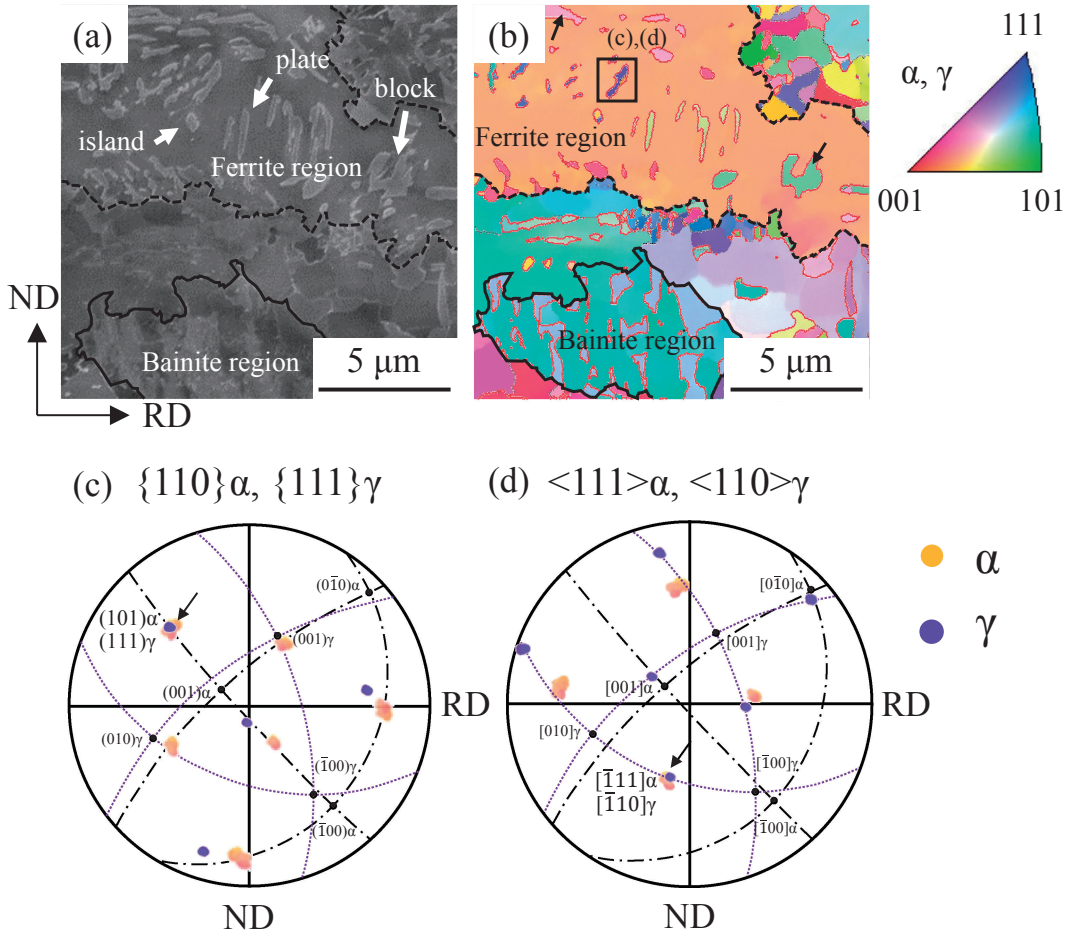

Fig. 1 Microstructure of as-received TRIP steel sheet on the TD plane: (a) secondary electron image, (b) IPF orientation map normal to RD, (c) pole figure of $\{011\}\alpha$ and $\{111\}\gamma$, and (d) pole figure of $\langle 111\rangle\alpha$ and $\langle 110\rangle\gamma$. The plate-like austenite marked by square in (b) represents the variant of $\{111\}\gamma$ satisfying K–S orientation relationship with $\{110\}\alpha$ of the ferrite matrix in (c) and (d). Arrows in (b) indicate the other two variants.

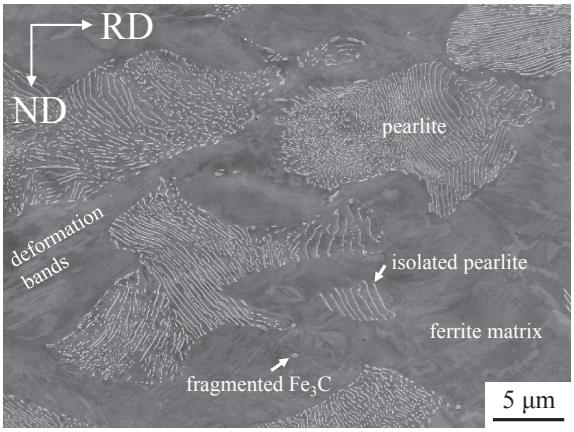

Fig. 2 Secondary electron image of fragmented cementite and isolated pearlite in the ferrite matrix for the cold-rolled TRIP steel sheet.

ferrite + austenite region with precipitation of austenite at deformation bands, isolated pearlites, and fragmented cementites, as each ferrite grain exhibited a homogeneous crystal orientation after the heat treatment. Subsequently, the austenite satisfied the K–S OR with the ferrite matrix. When austenite was reverse-transformed from martensite, the transformed austenite showed the same crystal orientation as the prior austenite grain.[14–16] The austenite satisfied the K–S OR with each martensite in the prior austenite grain. Hence, the variant selection mechanism is suggested,[15] where a single variant during the reverse transformation is selected according to the relaxation of the local residual stresses induced by martensitic transformation.[16] As no residual stress existed in the ferrite matrix, the austenite could be precipitated by satisfying the K–S OR with the ferrite matrix by reducing the interfacial energy between ferrite/austenite. The twenty-four variants of reverted austenite satisfying the K–S OR with the ferrite matrix revealed the same interfacial energy between them. Therefore, the retained austenite in the ferrite matrix was chosen to be any variant such that austenite grains with different crystal orientations were dispersed in the ferrite grain.

3.3 Transformation of retained austenite in ferrite grain

Figure 3 shows the IPF orientation maps of ferrite phases and misorientation profile across the boundaries between the ferrite and the austenite in an area with 0% ((a), (d)), 4% ((b), (e)), and 8% ((c), (f)) strains in tension at 193 K. The crystal orientation coordinate of the ferrite phase is parallel to the tensile direction, and the gray color area in Figs. 3(a)–(c) is fitted to austenite phase. The arrows from S to F in Figs. 3(a)–(c) represent the misorientation analysis lines for Figs. 3(d)–(f), respectively. Under 0% strain, the austenite

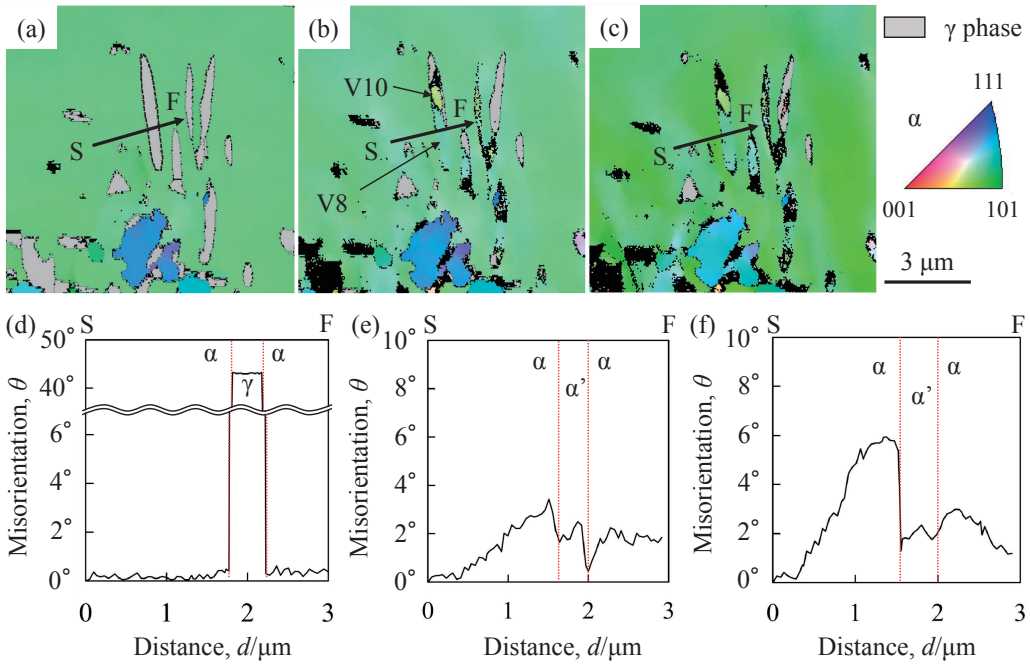

Fig. 3 Transformation of austenite in the ferrite matrix during an interrupted tensile test at 193 K: IPF orientation maps of α or α' phase at (a) 0% strain, (b) 4% strain, and (c) 8% strain, and (d)–(f) line profiles of misorientation along the arrows indicated in (a)–(c), respectively.

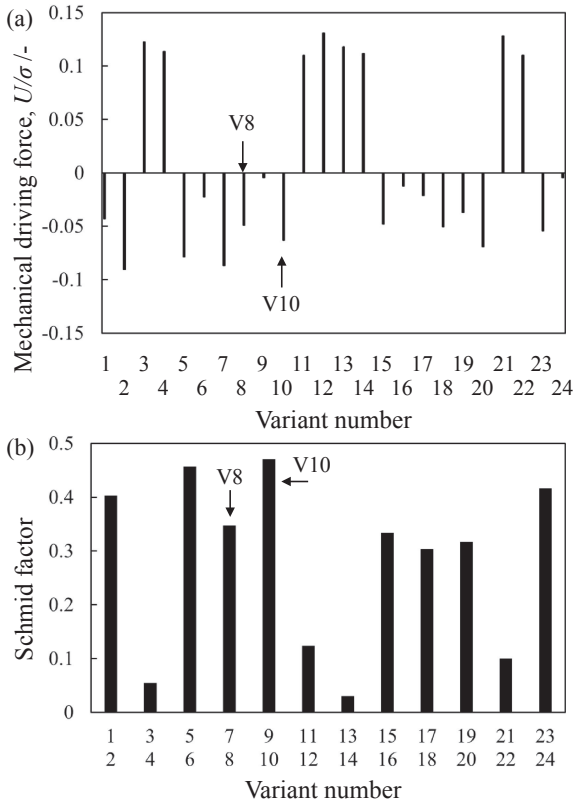

Fig. 4 Mechanical driving force (a) and Schmid factor (b) of twenty-four K–S variants for the retained austenite shown in Fig. 3(b). The orientation of the variant V8 was the same as that of the ferrite matrix, but the orientation of V10 was different.

grains were distributed in the ferrite matrix and they satisfied the K–S OR with the ferrite as shown in Fig. 3(a). Under 4% strain, a part of a retained austenite was transformed to martensite as shown in Fig. 3(b), and two kinds of variants, V8 and V10, were identified as presented in Table 1. Figure 4

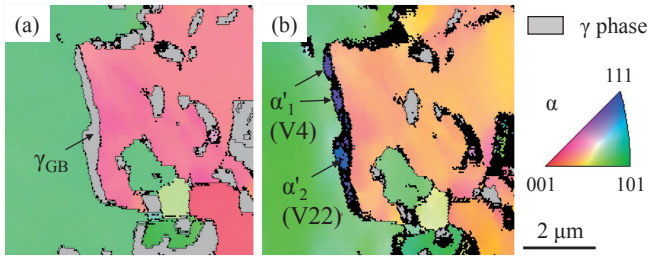

Fig. 5 Transformation of austenite at the α grain boundary during an interrupted tensile test at 193 K: IPF orientation maps of α or α' phase at (a) 0% strain and (b) 8% strain.

summarizes the mechanical driving force and Schmid factor of individual variants in the retained austenite analyzed in Fig. 3(b). The variant V8 was dominant and its orientation was the same as that of the ferrite matrix. No clear boundaries between the ferrite matrix and martensite were detected as shown the misorientation profile in Fig. 3(e). Such martensitic transformation commonly appeared in ferrite grains at the both the specimen surface and interior regardless of the test temperatures. Notably, the variant matching the ferrite matrix orientation was predominantly chosen, even though it revealed low mechanical driving force and/or it did not have the highest Schmid factor. It suggests that the influence of reduction of the interfacial energy between ferrite and martensite was predominant rather than that of the mechanical driving force or the reduction of energy owing to the choice of the primary or secondary slip plane.

Further, a small part of retained austenite was transformed by another variant with a high Schmid factor and low mechanical driving force as shown in Fig. 3(b). The variant V10 in Fig. 3(b) exhibits different orientation from the ferrite matrix, but had the highest Schmid factor (= 0.47). Thus, there is a possibility to operate the variant selection due to slip plane worked for the retained austenite in ferrite matrix.

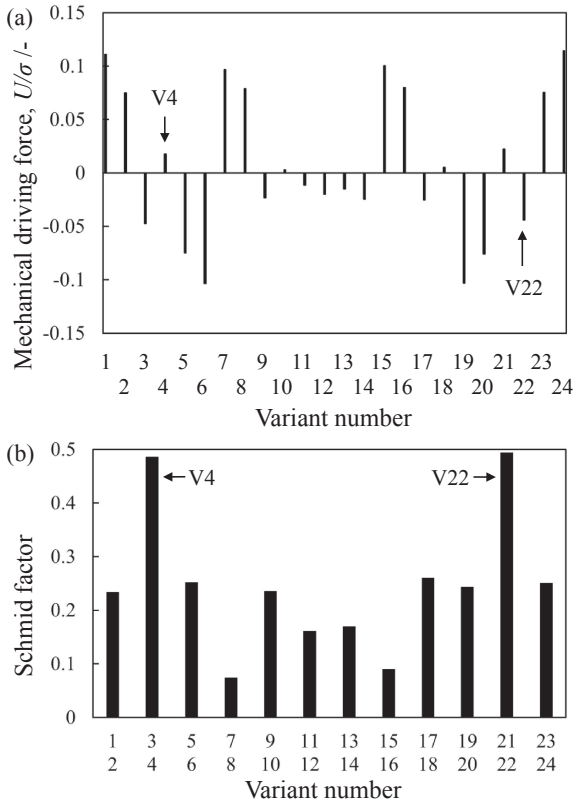

Fig. 6 Mechanical driving force (a) and Schmid factor (b) of twenty-four K–S variants for the retained austenite shown in Fig. 5(b). The variants of α'_1 and α'_2 were V4 and V22, respectively.

Under 8% strain, almost all the retained austenite was transformed to martensite as shown in Fig. 3(c), and thereafter, most of the martensite showed the same crystal orientation as the ferrite matrix. The misorientation in the ferrite matrix around the martensite was higher with the increase in strain as shown in Figs. 3(d)–(f), which indicated that the strain was concentrated at the ferrite/martensite boundaries in the ferrite matrix. Thus, the transformed martensite may act as a harder phase in the ferrite matrix.

3.4 Transformation of retained austenite at ferrite grain boundary

The retained austenite at ferrite grain boundaries, γ_{GB}, satisfied the K–S OR with ferrite grain on either side as shown in the grain on the right-hand side (pink color) in Fig. 5(a). However, the martensite transformed from the γ_{GB} showed different orientation with the ferrite grains on both sides. Further, the γ_{GB} was transformed to martensite with two types of variants, α'_1 (V4) and α'_2 (V22), in Fig. 5(b), where both the variants exhibited the highest Schmid factor ($\geqq$0.48) as shown in Fig. 6(b) and low mechanical driving force as shown in Fig. 6(a). Most of γ_{GB} was transformed to martensite with the variant showing the highest Schmid factor in the primary slip system, {111}-⟨110⟩, of individual austenite. When the variant matching the orientation of ferrite on either side was chosen, the martensite at the ferrite grain boundary developed a boundary with the ferrite on the other side, and achieved less reduction in the interfacial energy than that in the ferrite matrix. Therefore, the variant achieving the highest Schmid factor in individual austenite may be predominantly chosen to introduce slip deformation rather than to reduce the interfacial energy.

4. Conclusions

Deformation-induced martensite formed in individual reverted austenite satisfying Kurdjumov–Sachs orientation relationship with the ferrite matrix was characterized after tensile straining. The austenite was distributed in the ferrite matrix and at the grain boundaries. The major conclusions are summarized as follows:

(1) The austenite distributed in the ferrite matrix was predominantly transformed with the variant matched to the ferrite matrix orientation, even though the variant revealed low mechanical driving force and/or it did not have the highest Schmid factor. The influence of the reduction of interfacial energy between ferrite and martensite was predominant. The transformed martensite acted as a harder phase in the ferrite matrix and contributed to the strengthening of the present steel.

(2) The austenite at the ferrite grain boundaries was transformed to martensite owing to stress accommodation. The variant achieving the highest Schmid factor in individual austenite was predominantly chosen to introduce slip deformation rather than to reduce the interfacial energy.

REFERENCES

1) M. Takahashi: Nippon Steel Technical Report 88 (2003) 2–7.
2) K. Sugimoto, M. Kobayashi and S. Hashimoto: Metall. Trans. A **23** (1992) 3085–3091.
3) K. Sugimoto, M. Misu, M. Kobayashi and H. Shirasawa: ISIJ Int. **33** (1993) 775–782.
4) A. Itami, M. Takahashi and K. Ushioda: ISIJ Int. **35** (1995) 1121–1127.
5) G.K. Tirumalasetty, M.A. van Huis, C. Kwakernaak, J. Sietsma, W.G. Sloof and H.W. Zandbergen: Acta Mater. **60** (2012) 1311–1321.
6) J.R. Patel and M. Cohen: Acta Metall. **1** (1953) 531–538.
7) G. Miyamoto, N. Iwata, N. Takayama and T. Furuhara: Acta Mater. **60** (2012) 1139–1148.
8) G. Kurdjumov and G. Sachs: Ztsch. Phy. **64** (1930) 325–343.
9) S. Morito, H. Tanaka, R. Konishi, T. Furuhara and T. Maki: Acta Mater. **51** (2003) 1789–1799.
10) S. Takaki, K. Fukunaga, J. Syarif and T. Tsuchiyama: Mater. Trans. **45** (2004) 2245–2251.
11) Y. Matsuoka, T. Iwasaki, N. Nakada, T. Tsuchiyama and S. Takaki: ISIJ Int. **53** (2013) 1224–1230.
12) L. Cheng, A. Bottger, Th.H. de Keijser and E.J. Mittemeijer: Scr. Metall. Mater. **24** (1990) 509–514.
13) T. Furuhara, H. Kawata, S. Morito, G. Miyamoto and T. Maki: Metall. Mater. Trans. A **39** (2008) 1003–1013.
14) Y. Tomota, W. Gong, S. Harjo and T. Shinozaki: Scr. Mater. **133** (2017) 79–82.
15) T. Shinozaki, Y. Tomota, T. Fukino and T. Suzuki: ISIJ Int. **57** (2017) 533–539.
16) N. Nakada, T. Tsuchiyama, S. Takaki and S. Hashizume: ISIJ Int. **47** (2007) 1527–1532.